Stem Cell Reports
Article
OPEN ACCESS

SHOX2 Overexpression Favors Differentiation of Embryonic Stem Cells into Cardiac Pacemaker Cells, Improving Biological Pacing Ability

Vittoria Ionta,[1,2,4] Wenbin Liang,[1,4] Elizabeth H. Kim,[1] Reza Rafie,[1] Alessandro Giacomello,[2] Eduardo Marbán,[1] and Hee Cheol Cho[1,3,*]
[1]Cedars-Sinai Heart Institute, Los Angeles, CA 90048, USA
[2]Sapienza University of Rome, Rome 00161, Italy
[3]Departments of Biomedical Engineering and Pediatrics, Emory University, Atlanta, GA 30322, USA
[4]Co-first author
*Correspondence: heecheol.cho@emory.edu
http://dx.doi.org/10.1016/j.stemcr.2014.11.004

SUMMARY

When pluripotency factors are removed, embryonic stem cells (ESCs) undergo spontaneous differentiation, which, among other lineages, also gives rise to cardiac sublineages, including chamber cardiomyocytes and pacemaker cells. Such heterogeneity complicates the use of ESC-derived heart cells in therapeutic and diagnostic applications. We sought to direct ESCs to differentiate specifically into cardiac pacemaker cells by overexpressing a transcription factor critical for embryonic patterning of the native cardiac pacemaker (the sinoatrial node). Overexpression of *SHOX2* during ESC differentiation upregulated the pacemaker gene program, resulting in enhanced automaticity in vitro and induced biological pacing upon transplantation in vivo. The accentuated automaticity is accompanied by temporally evolving changes in the effectors and regulators of Wnt signaling. Our findings provide a strategy for enriching the cardiac pacemaker cell population from ESCs.

INTRODUCTION

Since their first derivation (Thomson et al., 1998), embryonic stem cells (ESCs) have been validated to faithfully recapitulate early cardiogenesis (Boheler et al., 2002; Van Vliet et al., 2012) and touted for their potential as an unlimited source of de novo cardiomyocytes for replacement of diseased myocardium (Kehat et al., 2001). While the most commonly pursued therapeutic goal has been to boost contractile function, ESC-derived cardiac cells may also be useful as alternatives to electronic pacemakers (Cho and Marbán, 2010); we and others have exploited the automaticity of ESC-derived cardiomyocytes to create biological pacemakers (Kehat et al., 2004; Xue et al., 2005). The risk of teratoma may be diminished by technical refinements to increase general yield of ESC-derived cardiomyocytes (Dubois et al., 2011; Kattman et al., 2011; Nunes et al., 2013) and by attaining a "pure" cardiomyocyte population post-differentiation (Dubois et al., 2011; Hattori et al., 2010). An outstanding issue, however, remains in the innate heterogeneity of ESC-derived (or any pluripotent stem cell) cardiac cells. The action potential (AP) profiles of de novo cardiomyocytes vary considerably from ventricular/atrial myocyte-like to nodal/Purkinje-like (He et al., 2003; Kolossov et al., 2005; Maltsev et al., 1993; Zhang et al., 2009). Such heterogeneity could result in unpredictable biological pacemakers, as reported in a subset of spontaneously contracting embryoid bodies (EBs) in which the beating rate either ceased or accelerated over time (Mandel et al., 2012).

We set out to develop a way to instruct the ESCs to differentiate into a cardiac pacemaker subtype with a factor relevant to embryonic pacemaker development. Native cardiac pacemaker cells are anatomically confined in the sinoatrial node (SAN), a diminutive structure comprising just a few thousand genuine pacemaker cells (Bleeker et al., 1980). During embryonic development, cardiac pacemaker cells originate from a subset of progenitors distinct from the first (marked by *Nkx2.5*) and second (marked by *Isl1*) heart fields not only in their genetic makeup (Christoffels et al., 2010; Wiese et al., 2009), but also in their anatomic location (Bressan et al., 2013). However, an area of *Hcn4*-positive primordial SAN is reported to express *Isl1* (Mommersteeg et al., 2007), suggesting that second heart field progenitors may also contribute to the developing SAN. We have recently demonstrated that postnatal re-expression of an embryonic transcription factor, *Tbx18*, converts ventricular cardiomyocytes to pacemaker cells, recapitulating morphological as well as electrophysiological hallmarks of genuine SAN pacemaker cells (Kapoor et al., 2013). Elsewhere, transgenic overexpression of *Tbx3* has been shown to elicit ectopic rhythm in mouse atrial myocardium (Bakker et al., 2012). Noting the powerful capacity of embryonic transcription factors in determining the fate of cardiac cell subtype, we hypothesized that overexpression of a SAN-specific transcription factor may steer ESC differentiation toward pacemaker cell subtype. Here, we report that heterologous expression of *SHOX2* during early stages of mouse ESC (mESC) differentiation strongly favors a SAN-specific gene program,

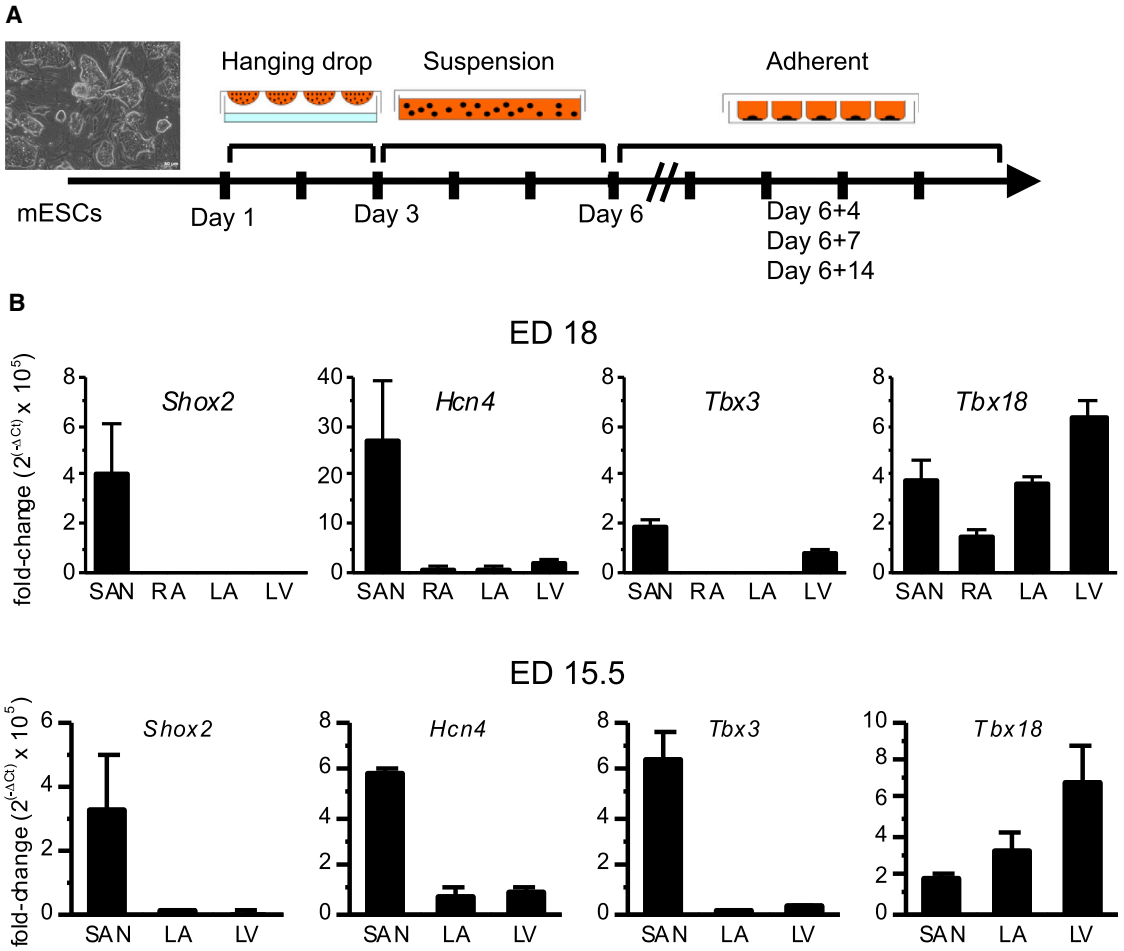

Figure 1. *Shox2* Is Specific to the Developing Mouse SAN

(A) A schematic diagram of cardiac differentiation protocol. mESCs were dissociated into single cells on day 1(D1) and cultured in suspension for 2 days in hanging drops and then 3 days on a nonadhering culture plate. On D6, the cells were plated on an adherent plate. The differentiating cells were characterized 4, 7, and 14 days from D6.

(B) Transcript expression levels of the transcription factors that govern cardiac pacemaker cell specification were quantified by real-time RT-PCR from microsurgically isolated SAN tissues from ED 18 mouse hearts (top). The bottom illustrates the gene expression level at ED 15.5. Expression analysis of RA was not performed at ED 15.5 because the tissue was too small to be reliably separated from the SAN. Purity of the SAN preparation is validated by robust *Hcn4* expression limited to the SAN (second from left). Data are represented as mean ± SEM. All experiments were performed in three independent biological replicates.

leading to enhanced pacemaker cell specification. The differentiated cells exhibit greater automaticity in vitro and perform biological pacemaker function when injected into the rat heart in vivo.

RESULTS

Shox2 Is Specific to Embryonic Development of the Cardiac SAN

mESCs were differentiated to form EBs by culturing them in suspension media for 6 days and then transferring them to adherent media (Wobus et al., 1991). The EBs were analyzed at three time points, based on the time course of electrophysiological maturation of mESC-derived cardiomyocytes (Maltsev et al., 1994): 4 days after transfer to adherent culture as an early time point of differentiation (D6+4), 7 days afterward (D6+7) as the mid phase of differentiation, and 14 days afterward (D6+14) as the terminal phase of differentiation (Figure 1A). A few transcription factors figure prominently in embryonic development of the SAN, notably the T box transcription factors *Tbx18* and *Tbx3* (Wiese et al., 2009), as well as the homeodomain transcription factor *Shox2*

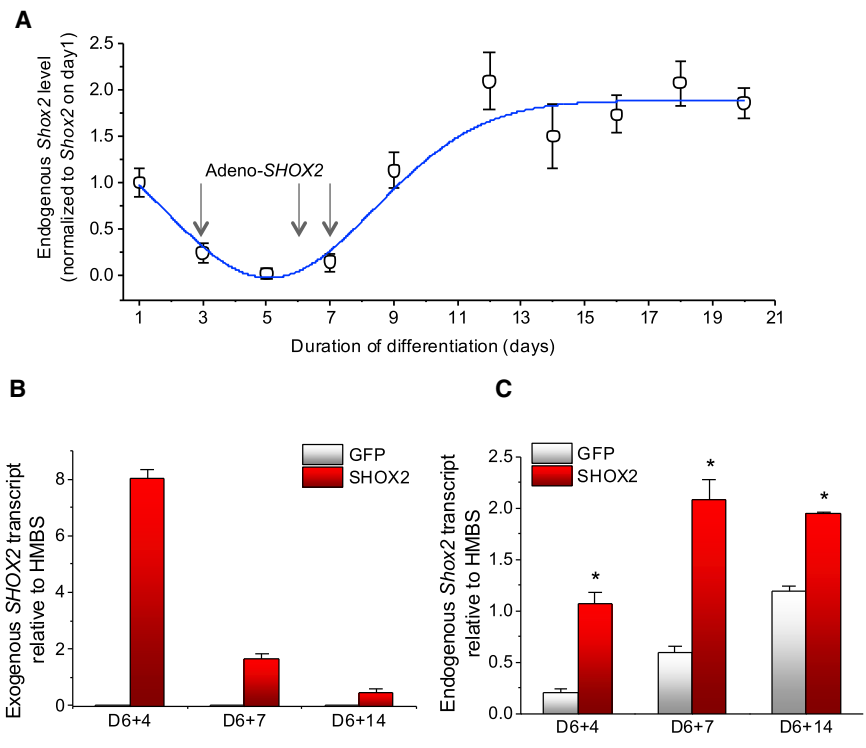

Figure 2. Exogenous Expression of Human *SHOX2* Increases Endogenous *Shox2* Expression

(A) Quantitative measurements of endogenous mouse *Shox2* expression throughout the differentiation stages indicate that its expression is at the lowest during the first 6 days of differentiation. In *SHOX2*-treated group, the differentiating cells are transduced with an adenoviral vector expressing human *SHOX2* on D3, D6, and D6+1 (D7) in order to maximize adenoviral somatic gene transfer. Experiments were performed on six independent mouse ESC cultures (i.e., six biological replicates).

(B) Human *SHOX2*-specific, quantitative PCR measurements of *SHOX2* over time. No PCR product was detected in the GFP-EB group, indicating the specificity of human *SHOX2* PCR primers.

(C) The level of endogenous *Shox2* expression is higher in the SHOX2-EB group compared with control in all three time points. Data are represented as mean ± SEM. All experiments were performed on three independent biological replicates.

See also Figure S1.

(Espinoza-Lewis et al., 2009). We reasoned that overexpression of one of these transcription factors could steer ESCs to differentiate into cardiac pacemaker cells. To this end, we sought to identify a gene highly specific to the developing mouse SAN. Quantitative measurements of the mRNA levels of these transcription factors reveal that *Shox2* expression is most specific to, and significant in, the SAN compared with the right atrium (RA), left atrium (LA), and left ventricle (LV) of the mouse heart at mouse embryonic day (ED) 18 (Figure 1B, top). The SAN-specific expression of *Shox2* closely follows that of *Hcn4*, a marker of SAN pacemaker cells. Initially, we anticipated that *Tbx18* expression might be the most specific to the SAN since mice deficient for *Tbx18* fail to form sinus horns (Christoffels et al., 2006), bolstered by our recent demonstration that *Tbx18* re-expression converts ordinary ventricular myocytes to native SAN-like induced pacemaker cells in vitro and in vivo (Kapoor et al., 2013). Yet, the present data indicate that *Tbx18* is comparably expressed between the SAN and all major chambers, including the right atrium (RA), left atrium (LA), and left ventricle (LV) at ED 18 (Figure 1B, top). This may be due to the abundance of $Tbx18^{+}$ proepicardial progenitor cells in the embryonic heart (Cai et al., 2008; Christoffels et al., 2009). Likewise, our data indicate that *Tbx3* is comparably expressed in the SAN and LV (Figure 1B), which may be due to its expression in ventricular conduction system (Bakker et al., 2008). Analogous results were obtained at an earlier embryonic development time point (ED 15.5; Figure 1B, bottom). Guided by these insights, we selected *Shox2* as the most SAN-specific transcription factor so as to boost SAN pacemaker cell-specific differentiation of the ESCs.

Exogenous *SHOX2* Expression Activates Endogenous *Shox2*

We set out to facilitate the pacemaker-specific gene program at a time when endogenous *Shox2* expression is low, from D3 to D7 (Figure 2A). To this end, we transduced the EBs with an adenoviral vector expressing human *SHOX2* at three time points (D3, D6, and D6+1). The use of human *SHOX2* allows specific transcript detection of endogenous mouse *Shox2* from exogenous human *SHOX2*. Human SHOX2 protein shares 98% amino acid sequence homology with mouse SHOX2 (Figure S1 available online), signifying likely bioactivity of human SHOX2 in a mouse context. The somatic gene transfer resulted in rapid expression of *SHOX2*, which waned steeply with time (Figure 2B), as expected from the transience of adenoviral vector-mediated somatic gene transfer (Michou et al., 1997; Tripathy et al., 1996). Importantly, exogenous *SHOX2* expression increased endogenous *Shox2* expression throughout the differentiation phases

(Figure 2C), suggesting stimulation of the pacemaker cell gene expression program.

SHOX2-EBs Exhibit Greater Automaticity with Concurrent Upregulation of Electrogenic Gene Program

We examined genes that play decisive roles for spontaneous diastolic depolarization as well as genes that underlie the propagation of electrical signals from cell to cell. Hyperpolarization-activated cyclic nucleotide-gated channel 4 (HCN4) is the molecular correlate of I_f in the SAN, which directly contributes to the linear rise of spontaneous depolarization during phase 4 of an AP (DiFrancesco, 2010; Yamamoto et al., 2006). Immunostaining of the whole EBs demonstrates that *SHOX2* expression heightens HCN4 channel expression compared with control (Figure 3A). Total HCN4 protein expression was twice higher in SHOX2-EBs compared with control throughout the stages of differentiation (Figure 3B, left and middle). Na^+-Ca^{2+}exchanger (NCX) couples spontaneous intracellular Ca^{2+} release events to voltage oscillations in SA nodal pacemaker cells (Lakatta and DiFrancesco, 2009). The NCX1 protein level increased 4-fold in SHOX2-EBs at the later stages of differentiation (Figure 3B, right; Figure S2).

The space constant at the core of the SAN is significantly lower than that of the neighboring atrial myocardium or the ventricles (<500 μm versus 1–2 mm, respectively) (Bonke, 1973). The high intercellular electrical resistance in the SAN allows its automaticity to propagate into the right atrium, which due to its highly hyperpolarized membrane potential would otherwise dissipate the electrogenic signals from the SAN (Joyner and van Capelle, 1986). The weak electrical coupling in the SAN pacemaker cells is mediated by a low-conductance gap junction protein, CX45, while the chamber myocardium predominantly expresses a large-conductance gap junction, CX43 (Jansen et al., 2010). *SHOX2* overexpression increased the transcript level of *Gja7*, the gene that encodes CX45, throughout the differentiation phases. This is complemented by an ~4-fold increase in CX45 protein expression (Figure 3C). Conversely, *SHOX2* overexpression decreased CX43 expression at the transcript (33% ± 5%, $p < 0.05$) and protein (30% ± 10%, $p < 0.05$) levels compared with control (Figure 3D). In order to gauge the extent of total cardiac myocyte differentiation, we examined the expression levels of pan-cardiac myocyte markers, cardiac troponin T (*Tnnt2*), and cardiac actin (*Actc1*), as well as *Nkx2-5*, a negative marker of SAN but positive for ventricular and atrial cardiomyocytes. Quantitative RT-PCR data demonstrate that the expression level of *Nkx2-5* is lower in SHOX2-EBs, while that of the pan-cardiac myocyte genes remains similar (Figure S3). The data indicate that the total cardiac differentiation efficiency remains similar in SHOX2-EBs and EBs transduced with a green fluorescent protein (GFP-EBs). Furthermore, the increased automaticity in SHOX2-EBs is likely to be a direct result of heightened pacemaker cell differentiation at the expense of diminished ventricular cardiomyocyte content. Thus, exogenous *SHOX2* expression upregulates a number of electrophysiological hallmarks of SAN pacemaker cells during cardiac differentiation of ESCs.

To quantify the automaticity of SHOX2-EBs, we scored the number of spontaneously beating EBs and the number of individual beating foci in each EB. At the early stage of differentiation, the majority of SHOX2-EBs beat spontaneously, while the majority of GFP-EBs were quiescent (83% ± 7% versus 15% ± 6%, respectively, n = 7 independent experiments; Figure 4A, left). Over time, most of the GFP-EBs eventually began to beat (Figure 4A, left). Still, SHOX2-EBs exhibited more than twice the number of spontaneously beating foci within each beating EB compared with control, a pattern that persisted throughout differentiation (Figure 4A, right). The beating rates of the EBs were analyzed by recording extracellular field potentials (FPs) from the EBs on multielectrode arrays (MEAs) (Figure 4B). The beating rates of SHOX2-EBs were similar to those of control at the beginning of differentiation and then became significantly faster compared with control beyond the mid phase of differentiation (Figures 4C and 4D). Taken together, the data demonstrate that SHOX2-EBs develop greater numbers of pacemaker foci with faster beating rates and that the increased automaticity persists throughout differentiation.

SHOX2-EBs Function as a Biological Pacemaker after Transplantation In Vivo

Motivated by the greater automaticity of the SHOX2-EBs, we tested whether SHOX2-EBs could provide biological pacemaker function when implanted in vivo. We and others have previously demonstrated that spontaneously beating human ESC-derived EBs could electrically couple with and drive the beating of host myocardium upon implantation in vivo (Kehat et al., 2004; Xue et al., 2005). In those studies, spontaneously beating areas of several EBs were microsurgically dissected prior to injection so as to remove nonbeating areas, thereby maximizing the proportion of beating cardiac tissue to nonbeating cells. Here, we tested whether the increased automaticity in SHOX2-EBs suffices to provide biological pacemaker function even without microsurgical removal of nonbeating cells. To this end, 10–12 spontaneously beating GFP-EBs or SHOX2-EBs were randomly selected at D6+4 and directly injected into the left ventricular apex of the rat heart in vivo. Two to 4 days after in vivo transplantation, the heart was isolated and retrogradely perfused so that its electrical activity could be optically mapped. In sinus rhythm,

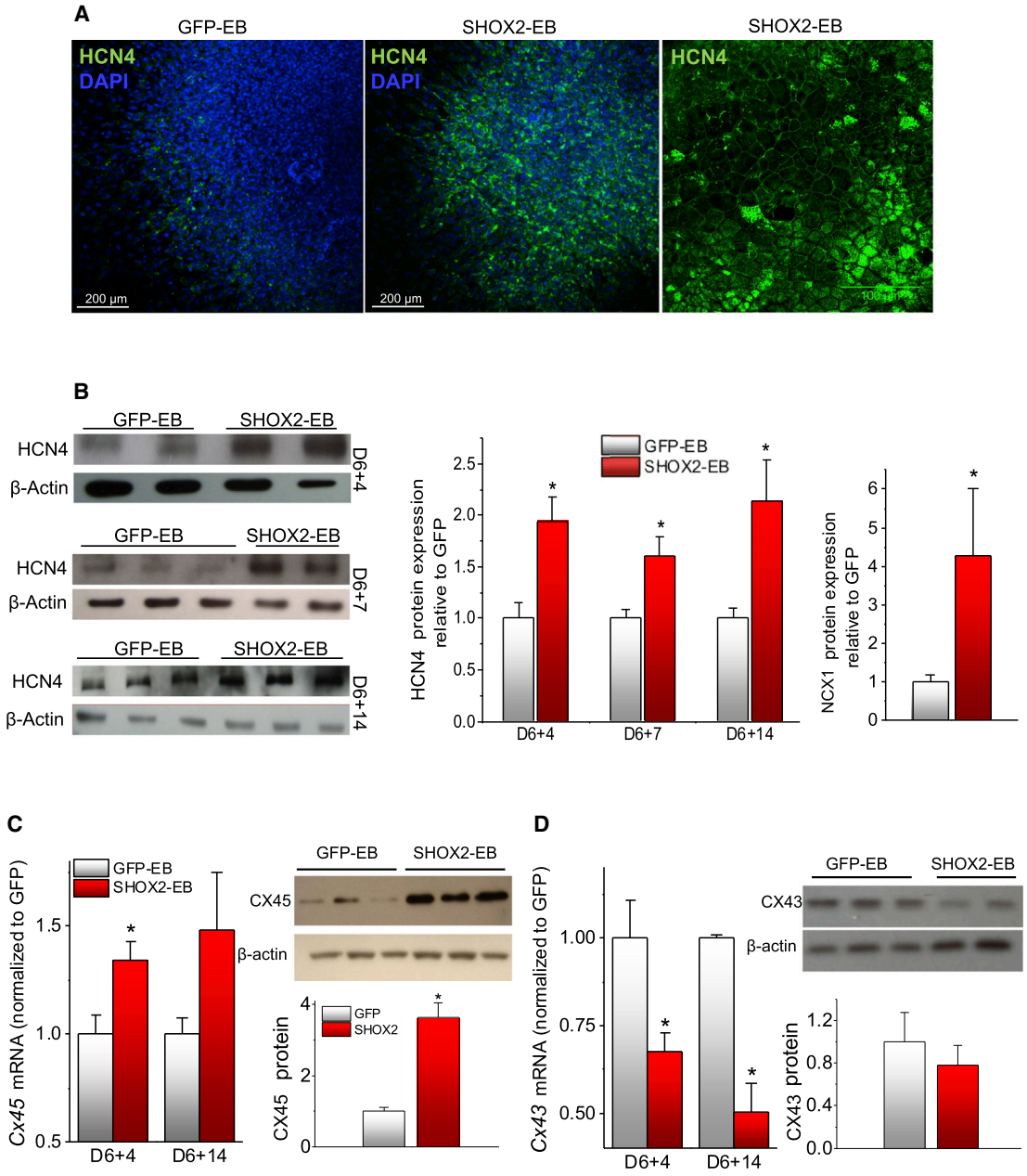

Figure 3. Changes to Ion Channel and Gap Junction Profiles in SHOX2-EBs Favor Automaticity

(A) Immunostaining images of GFP-EB (left) and SHOX2-EB (middle and right) with an antibody against HCN4 channel proteins. DAPI (blue), nuclear staining.

(B) Quantitative measurements of HCN4 (left and middle) and NCX1 (right) protein levels. D6+14 for NCX1.

(C) Transcript (left) and protein (right) level measurements of Cx45 in GFP-EBs and SHOX2-EBs. Protein level was determined with D6+14 samples.

(D) Transcript (left) and protein (right) level measurements of Cx43 in GFP-EBs and SHOX2-EBs. The protein level was determined with D6+14 samples. Data are represented as mean ± SEM. All experiments were performed on three independent biological replicates.

See also Figures S2 and S3.

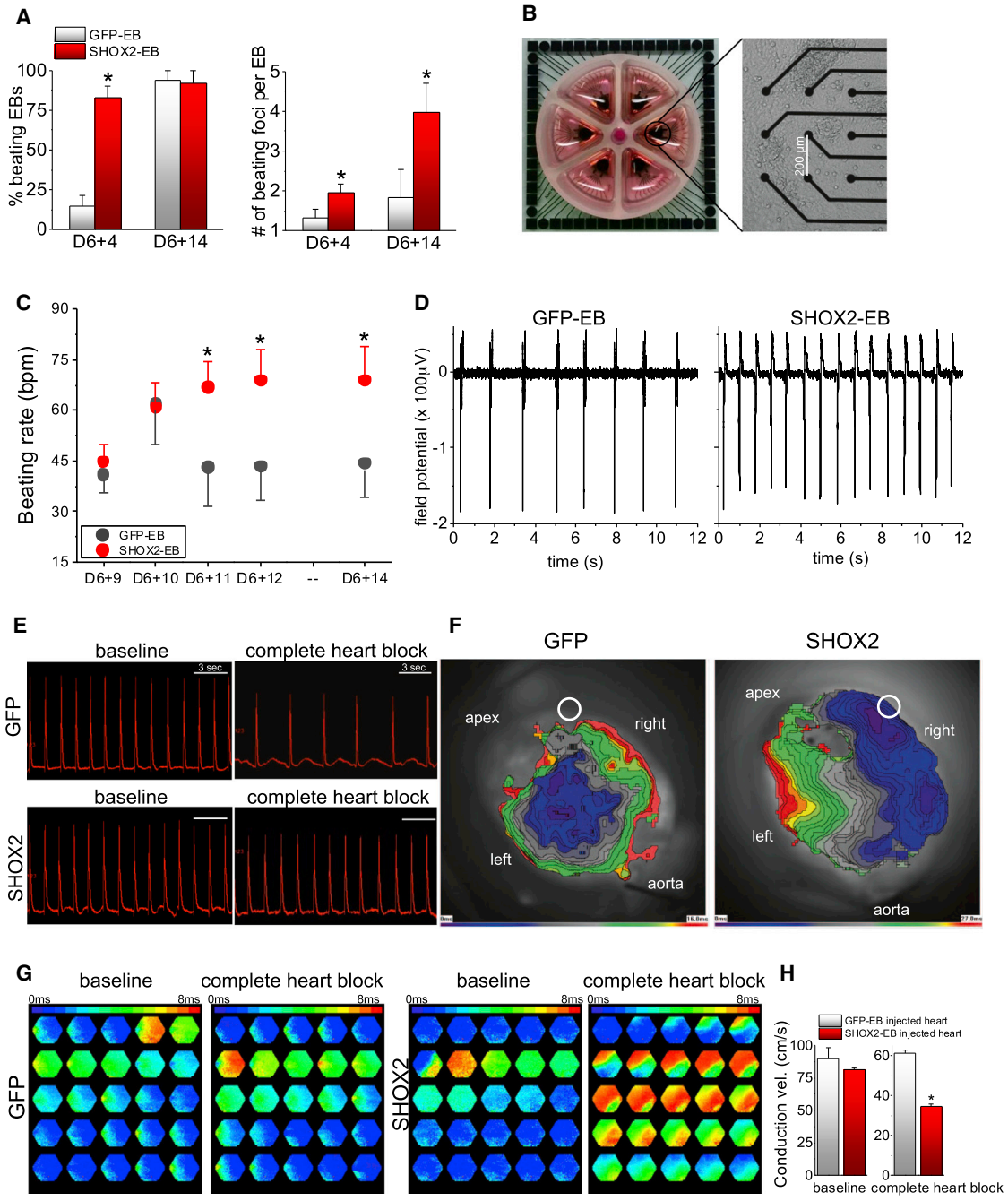

Figure 4. SHOX2-EBs Exhibit Intensified Automaticity In Vitro and Function as Biological Pacemakers when Implanted In Vivo

(A) The percentages of spontaneously contracting EBs were measured at D6+4 and D6+14 (left) by direct visualization. More than one beating focus could be detected in some EBs, and thus, the number of spontaneously beating foci per EB was measured at the same time points (right).

(B) The spontaneous beating rates were measured by culturing the EBs in MEAs and measuring the extracellular FPs from the GFP-EBs and SHOX2-EBs. Shown is a six-well MEA (left) in which two to three EBs were cultured per well (right).

(C) The average beating rates were measured at five time points by recording the spontaneous FPs for 20 min at 37°C in normal Tyrode's (n > 10 for each data point).

(D) Representative raw FP traces are shown for a GFP-EB and a SHOX2-EB at D6+14.

(E) Whole-heart optical mapping recordings were performed on the rat hearts injected with GFP-EBs or SHOX2-EBs in vivo 2–3 days prior to the heart harvest. Raw AP traces reported as di-8-ANNEPS signal from one photodiode (123) are shown before (baseline) and after

(legend continued on next page)

hearts injected with either GFP-EBs or SHOX2-EBs exhibited similar heart rates at room temperature (Figure 4E, "baseline"). Then complete heart block was implemented by surgically disrupting both the SA and atrioventricular nodes to unleash potential biological pacemaker activity. Afterward, control hearts injected with GFP-EBs exhibited slow junctional rhythms of 34 ± 2 beats per minute (bpm) (n = 4). In contrast, the SHOX2-EB-injected hearts exhibited a significantly higher ventricular rate (44 ± 3 bpm, n = 4, $p < 0.05$). Since the SHOX2-EBs were injected in the ventricular myocardium, heartbeats initiated from the injection site are expected to propagate more slowly than a junctional rhythm, which travels via the fast secondary conduction system. Under sinus rhythm, conduction velocities from hearts implanted with SHOX2-EBs were comparable to those from the hearts injected with GFP-EBs, with rapid spreading of the depolarization wave front. After the induction of complete heart block, conduction velocity slowed significantly in the SHOX2-EB-injected hearts, as anticipated for a wave front propagating through nonspecialized myocardium (Figures 4F and 4G; Movies S1 and S2). In contrast, the conduction velocity of GFP-EB-injected hearts did not change in complete heart block (Figure 4H, bar graphs). Electrical coupling between the donor and the host myocardium is evidenced by the presence of gap junction proteins at the interface between SHOX2-EBs and the rat ventricular myocardium (Figure S4). Taken together, the data indicate that SHOX2-EBs, but not GFP-EBs, function as biological pacemakers when the EBs were randomly selected and injected into the left ventricular apex of the rat heart.

Electrophysiology of Single Cells Isolated from SHOX2-EBs

In order to investigate the pacemaker phenotype of SHOX2-EBs at the single-cell level, we characterized APs from freshly isolated, spontaneously beating cells from SHOX2-EBs or GFP-EBs. The majority (62%) of single cells isolated from SHOX2-EBs exhibit a pacemaker-like AP profile, while 74% of the single cells isolated from GFP-EBs exhibit ventricular/atrial-like APs (Figures 5A and 5B). Single cells from SHOX2-EBs also fired APs at a higher rate than control cells (Figure 5C, left). The mean amplitude of spontaneous APs was lower in SHOX2-EB cells (Figure 5C, second from left), consistent with the lower I_{Na} density in genuine SAN pacemaker cells (Kapoor et al., 2013). Action potential duration (APD) was shorter, and each AP was preceded by faster phase 4 depolarization in SHOX2-EB cells compared with control (Figure 5C, right two panels). The density of I_f, a key contributor to spontaneous phase 4 depolarization (Lakatta and DiFrancesco, 2009), was significantly higher in SHOX2-EB cells compared with control (Figures 5D and 5E). Thus, SHOX2-EB cells more often display SAN-like AP parameters. Furthermore, the spontaneously beating single cells from both groups responded predictably to adrenergic stimulation and muscarinic challenge (Figures 5F and 5G), demonstrating their responsiveness to neurohumoral input.

DISCUSSION

Shox2 is indispensable for proper formation and development of the SAN. *Shox2* null/null mouse embryos exhibit severe hypoplasia of the SAN accompanied by an aberrant expression of chamber cardiomyocyte-specific markers in the SAN (Blaschke et al., 2007; Espinoza-Lewis et al., 2009). Mouse *Shox2* is first detected at ED8.5 in the posterior region of the developing heart tube, and its expression terminates by ED 13.5, being restricted to the cardiac conduction system (Blaschke et al., 2007; Espinoza-Lewis et al., 2009). Genetic ablation of *Shox2* results in slowed contraction rate in mESC-derived EBs (Hashem et al., 2013). Here, we demonstrate that transient and heterologous expression of *SHOX2* greatly increases the percentage of spontaneously beating EBs, the number of beating foci in each EB, and the EB contraction rate compared with control (Figures 4A–4D). The enhanced automaticity correlates directly with more $HCN4^+$ cells present in SHOX2-EBs compared with control (Figure 3A). Direct injection of SHOX2-EBs

complete heart block. Upon complete heart block, the hearts injected with SHOX2-EBs demonstrated significantly higher heart rate compared to control (right).

(F) Optically recorded isochronal maps superimposed on the whole-heart injected with GFP-EBs (left) or SHOX2-EBs (right). A white circle indicates the EB implantation site, and the aorta is positioned at the bottom of the image. The anterior side of the heart was positioned to face the CMOS camera. Note the differences in the time scale of the isochronal map; 16 and 27 ms for end-to-end AP propagation for GFP-heart and SHOX2-heart, respectively.

(G) Frame-by-frame analysis of the optical mapping exhibiting AP propagation. The data illustrate slower AP propagation upon complete heart block in the hearts injected with SHOX2-EBs compared with control. Each hexagonal frame, recorded with a photodiode array, measures to a small area of about 8 mm^2 on the heart.

(H) The conduction velocity of SHOX2-EB injected hearts was significantly slower than that from the control heart upon complete heart block. Data are represented as mean ± SEM. All experiments were performed on three independent biological replicates.

See also Figure S4 and Movies S1 and S2.

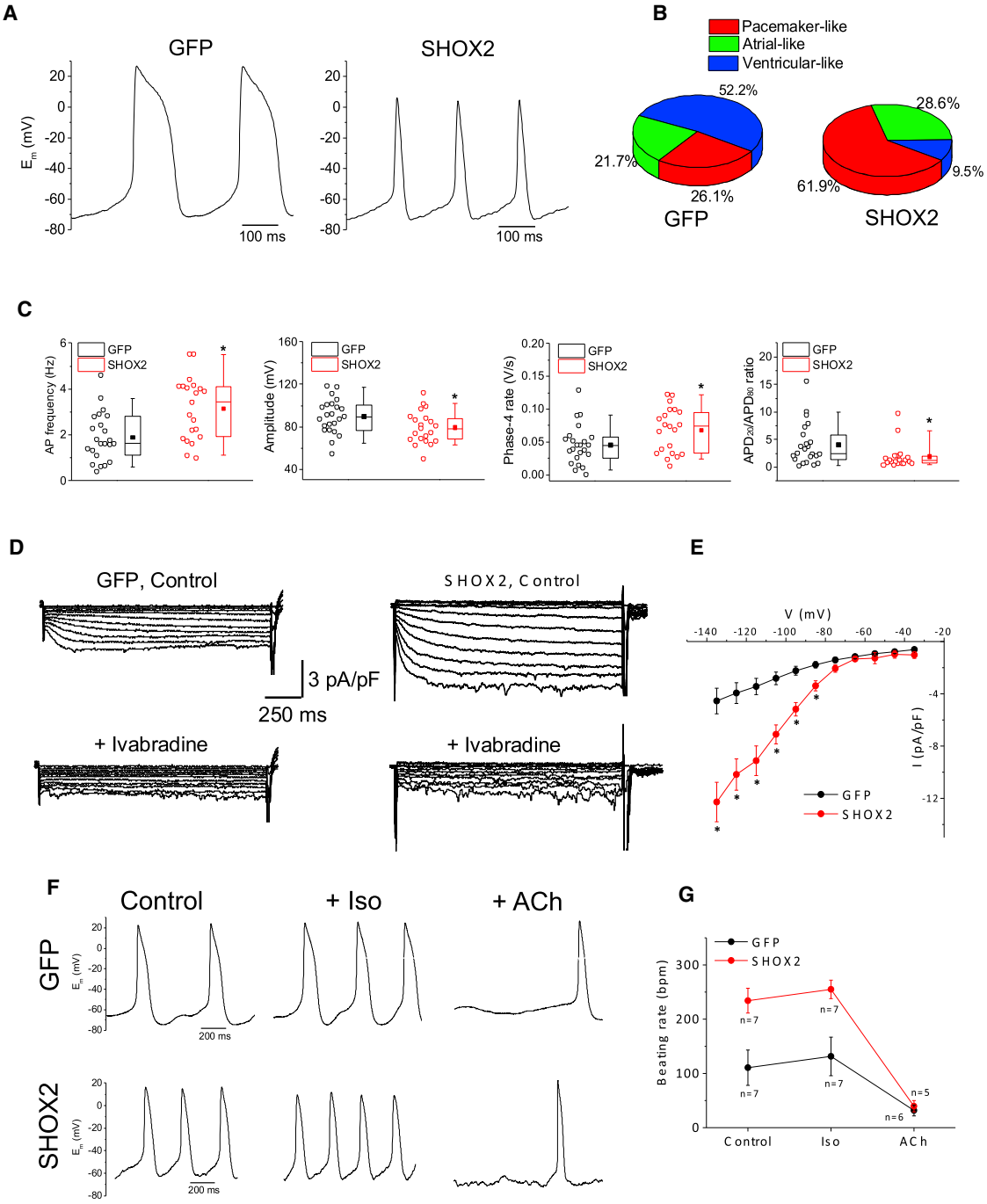

Figure 5. Single-Cell Electrophysiology of SHOX2-EBs Demonstrate SAN Pacemaker Cell-like Electrophysiology

(A) Representative raw traces of APs recorded from spontaneously-beating single cells from GFP-EBs (left) or SHOX2-EBs (right).

(B) Percentage of cells with pacemaker-like, atrial-like, or ventricular-like APs in GFP (n = 23) and SHOX2 (n = 21) groups.

(C) Comparison of AP parameters (from left to right): spontaneous beating rate, amplitude of the AP upstroke, spontaneous phase 4 diastolic depolarization rate, and ratio of AP duration at 20% repolarization (APD_{20}) to 80% repolarization (APD_{80}). *p < 0.05.

(D) Representative HCN ionic currents (I_f) recorded from a GFP-EB cell (left) and a SHOX2-EB cell (right). Lower panels show the inhibition of time-dependent currents upon addition of 10 μM ivabradine in the bath solution. HCN currents were recorded in normal Tyrode's solution containing 1 mM $BaCl_2$ in order to block contaminating inward rectifier K^+ currents. The I_f currents were elicited with a family of voltage steps from −135 mV to +35 mV for 1.5 s with 10 mV increment from a holding potential of −35 mV.

(legend continued on next page)

into the rat left ventricular apex created ectopic automaticity indicative of induced biological pacing at a rate faster than the junctional escape rhythm observed in hearts injected with GFP-EBs (Figure 4E). The enhanced automaticity is accompanied by increased expression of automaticity-promoting genes and gene products such as HCN4, NCX1, and CX45 (Figure 3).

As rationale for the timing of *SHOX2* overexpression, it may have been more logical to base it when *Shox2*-positive progenitors exist. In this regard, *Shox2* expression is detected as early as day 6 of differentiation (Hashem et al., 2013) in an mESC-derived EB system. This largely coincides with the time points of exogenous *SHOX2* overexpression (D3, D6, D7) in our study. It is notable that the beating rates of the GFP-EBs rise and then recede between D6+9 and D6+11 (Figure 4C). The majority of embryonic cardiac myocytes have the tendency to beat spontaneously but become more quiescent as they mature electrophysiologically (Pelleg et al., 1980). Likewise, the rapid decrease in the beating rates of GFP-EBs may be due to changes in their electrophysiological components, similar to the swift increase in I_{Na} density in differentiating, mESC-derived EBs (Maltsev et al., 1994). In contrast, the spontaneous beating rates remain high in SHOX2-EBs (Figure 4C), further supporting the notion that the superior automaticity of SHOX2-EBs is due to enhanced differentiation to pacemaker cells rather than to nonspecific deterioration of chamber cardiomyocytes.

Cardiac derivatives from ESCs consist of cardiomyocytes of atrial and ventricular phenotypes as well as pacemaker-like cells (Wobus et al., 1995). Because of the absence of specific extracellular epitopes, no live cell sorting method exists to purify pacemaker, ventricular, or atrial myocytes without genetic tagging. As such, the inherent heterogeneity of pluripotent stem cell-derived cardiomyocytes poses a critical impediment to therapeutic/diagnostic applications. For biological pacemaker applications, contaminating ventricular/atrial myocytes in the newly derived cardiac derivatives may compromise pacemaking activity from the implanted cells. Conversely, the presence of pacemaker cells may be arrhythmogenic if ESC-derived cardiomyocytes were to replace a large mass of damaged myocardium. Although implantation of human ESC-derived cardiomyocytes in the guinea pig hearts was shown to be antiarrhythmic (Shiba et al., 2012), delivery of the same cells in nonhuman primates resulted in premature ventricular contractions and ventricular tachycardia in all experimental animals (Chong et al., 2014).

As an in vitro diagnostic tool, induced pluripotent stem cell-derived cardiac myocytes have been proposed as an in vitro platform for drug screen for arrhythmic diseases such as Long QT syndrome (Itzhaki et al., 2011). However, the inherent heterogeneity of these cells, complicated by the fact that the derived cardiomyocytes are largely immature (Mummery et al., 2010; Mummery et al., 2012), may result in erroneous index of how a putative drug may react in atrial or ventricular myocardium. These concerns underscore the need for attaining subtype-specific populations of cardiomyocytes. Previous work by others has tried to address this by inducing pluripotent stem cells to cardiac pacemaker-like cells with various pharmacological agents (Kleger et al., 2010; Müller et al., 2012; Wiese et al., 2011). Here, we demonstrate that *SHOX2*-mediated pacemaker cell potentiation leads to heightened automaticity in the EBs and that the SHOX2-EBs provide biological pacemaker function upon transplantation into the rat myocardium in vivo. Implantation of the SHOX2-EBs was performed without microsurgical excision of nonbeating areas of the EBs, further highlighting the intensified automaticity in the SHOX2-EBs. The long-term potential of ESC-derived EBs as durable biological pacemakers is an important step toward clinical realization (Jung et al., 2014). However, we do not offer the present findings as a direct prelude to long-term biological pacing tools, but rather as insights into the progression of pacemaker cell development as they are reflected in the EB system.

Because embryonic development of the SAN occurs concurrently with the looping of the linear heart tube (Christoffels et al., 2004), major signaling motifs may impart a unique signature on the developing SAN from the general myocardium. Wnt signaling is indispensable for embryonic heart development (Schneider and Mercola, 2001) and can be manipulated to enrich the cardiomyocyte population from human ESCs (Lian et al., 2012; Willems et al., 2011). Since canonical Wnt signaling is necessary for maintaining mesenchymal precursors that later form the sinus horn (Norden et al., 2011), we looked for differential expression of Wnt ligands and regulators in SHOX2-EBs. On day 6+4 expression of noncanonical Wnt, ligands are mostly suppressed, while that of Wnt inhibitors are higher in SHOX2-EBs compared with control (Figure S5A),

(E) Current density-voltage relationships of GFP (black, n = 4) and SHOX2 (red, n = 5) groups. *p < 0.05.
(F) Representative APs of a GFP cell (top row) and a SHOX2 cell (bottom row) before (left) and after treatment with isoproterenol (Iso, 1 μM, middle) or acetylcholine (ACh, 50 nM, right).
(G) Summary of beating rate responses before and after treatment with isoproterenol or acetylcholine. Data are represented as mean ± SEM. All experiments were performed on three independent biological replicates.

but the expression pattern reverses later at D6+14 (Figures S5B and S5C). Inhibition of endogenous Wnt generally potentiates cardiac differentiation of ESCs (Kattman et al., 2011; Paige et al., 2010). In contrast, the expression of classical Wnt inhibitors such as *Dkk1*, *Sfrp4*, and *Wif1* is significantly downregulated in SHOX2-EBs at D6+4 (Figure S5C). The data point to antagonistic effects of Wnt signaling on cardiac myocyte subtype specification, manipulation of which may steer the ESCs to differentiate into a specific cardiac cell type.

EXPERIMENTAL PROCEDURES

Mouse ESC Culture

The mESC line, R1 (ATCC) was cultured in KnockOut Dulbecco's modified Eagle's medium supplemented with 15% KnockOut Serum Replacement, 2 mM L-glutamine, 50 units/ml penicillin, 50 μg/ml streptomycin, 1% MEM nonessential amino acids, and β-mercaptoethanol. The mESCs were kept undifferentiated by culturing them on confluent monolayers of mitomycin C-treated primary mouse embryonic fibroblasts (Millipore) and by adding purified recombinant mouse leukemia inhibitory factor (ESGRO, 1,000 units/ml; Millipore). Cells were maintained at 37°C in a humidified atmosphere of 5% CO_2.

Molecular Cloning and Adenovirus Purification

The human *SHOX2* gene with a C-terminal myc/FLAG tag was excised from pCMV6-Tbx18 (Origene) by digestion with FseI and SalI and then subcloned into a NotI- and XhoI-digested lentiviral expression vector with the desired reporter gene, pLVX-IRES-ZsGreen1 (Clontech) to create pLV-Tbx18-IRES-ZsGreen. The recombinant target gene was then introduced to an adenovirus vector backbone by Gateway recombination cloning using Gateway-adapted vectors (Invitrogen). LR recombination reaction was performed between the entry clone and the destination vector, pAd/CMV/V5-DEST, to generate the desired adenoviral expression construct, pAd-CMV-SHOX2-IRES-ZsGreen. Positive constructs were verified to have the correct target gene by DNA sequencing (Laragen). The expression constructs were digested with PacI to expose inverted terminal repeats before transfecting into 293A cells to produce adenoviral stocks. Adenoviruses were amplified and affinity-column-purified using Adenopure kit (Puresyn) and stored at −80°C.

Differentiation of mESCs and Adenoviral Transduction

The cardiac differentiation media are composed of Iscove's modified Dulbecco's medium with Glutamax, ESC qualified fetal bovine serum (Embryomax, 20%), minimal essential media nonessential amino acids (1%), penicillin (50 units/ml), streptomycin (50 μg/ml), and β-mercaptoethanol (0.1 mM). On day 1, mESCs were dissociated with 0.05% trypsin-EDTA. Single ESCs were cultured in hanging drops (at 400 cells per 20 μl) to form EBs for 2 days. On day 3, the EBs were transferred to ultra-low-attachment dishes (Corning) and transduced either with an adenoviral vector expressing *SHOX2* (Ad-SHOX2-IRES-GFP) or a control vector (Ad-GFP) at a multiplicity of infection (MOI) of 500. At day 6, control and treated EBs were plated onto gelatin-coated culture dishes. The EBs were transduced again at day 6 and D6+1 with the same MOI as at day 3 in order to maximize somatic gene transfer.

Scoring the Beating EBs

The numbers of spontaneously beating EBs and of beating foci per EB were counted under a bright-light microscope in a temperature- and CO_2-controlled chamber. The position of each beating cluster was marked to avoid double counting.

RNA Extraction, Quantitative Real-Time PCR, and Wnt PCR Array

Total RNA was extracted from the embryonic mouse heart tissues with RNeasy Mini Kit (QIAGEN) followed by DNase treatment. RNA concentration was assessed by spectrophotometry (NanoDrop; Thermo Scientific). Real-time quantitative PCR was performed with the Taqman One Step PCR kit (Applied Biosystems) according to the manufacture's recommended protocol. Primers used for quantitative RT-PCR were all from Applied Biosystems. Housekeeping genes such as glyceraldeyde-3 phosphate dehydrogenase and Hydroxymethylbilane synthase (HMBS) were employed as internal control. For PCR array analyses, total RNA (1 μg) was reverse transcribed into cDNA using the RT^2 First Strand Kit (SA Biosciences). The resulting cDNA was analyzed using the Wnt Pathway PCR Array (catalog number PAMM-043; SA Biosciences). All quantitative PCR reactions were performed on an ABI 7900 HT fast Real-Time PCR System (Applied Biosystems). All experiments were performed in triplicates with three biological replicates. All primer sets used for quantitative RT-PCR (qRT-PCR) were purchased from Applied Biosystems (Table 1).

Western Blot Analysis

Whole-cell lysates were harvested with RIPA Buffer (Thermo Scientific) containing protease inhibitors (HALT Protease Cocktail; Pierce). Protein concentrations were determined with bicinchoninic acid protein assay (MicroBCA Kit; Pierce). Samples were loaded onto 12% SDS-PAGE, and the separated proteins were transferred to a polyvinylidine fluoride membrane. Blots were incubated overnight at 4°C with the primary antibodies against HCN4 (Abcam), Connexin-45(CX45; Invitrogen), Connexin-43 (CX43; Sigma-Aldrich), and Na^+/Ca^{2+} exchanger (NCX1; Abcam). The primary antibodies were detected using horseradish peroxidase-conjugated secondary antibodies raised in appropriate species, followed by chemiluminescence detection (Pico Chemiluminescence Substrate; Pierce). Protein loading was controlled by reprobing the membranes with monoclonal anti-β-actin antibody (Sigma-Aldrich).

Immunocytochemistry

Whole EBs were fixed using 4% paraformaldehyde, washed with PBS, and permeabilized with 0.1% Triton X-100. Fixed cells were blocked with 5% normal donkey serum overnight at 4°C. The EBs were then incubated with primary antibodies for HCN4 (Abcam) and a secondary antibody conjugated with Alexa Fluor 488

Table 1. Primer Sets for Quantitative PCR

	Catalog Identification	Interrogated Sequence (RefSeq)	NCBI Chromosome Location	Exon Boundary	Amplicon Length
Human *SHOX2*	Hs00243203_m1	NM_001163678.1	chromosome 3: 157813800–157823952	2–3	129
Mouse *Shox2*	Mm00443183_m1	NM_013665.1	chromosome 3: 66973266–66981771	1–2	97
Mouse *Tbx3*	Mm01195726_m1	NM_011535.3	chromosome 5: 119670669–119684601	7–8	65
Mouse *Tbx18*	Mm00470177_m1	NM_023814.4	chromosome 9: 87702800–87731260	6–7	64
Mouse *Nkx2.5*	Mm00657783_m1	NM_008700.2	chromosome 17: 26838665–26841565	1–2	117
Mouse *Actc1*	Mm01333821_m1	NM_009608.3	chromosome 2: 114047289–114052811	3–4	62
Mouse *TnnT2*	Mm01290256_m1	NM_001130174.2	chromosome 1: 135836386–135852261	8–9	110
Mouse *Hmbs*	Mm01143545_m1	NM_001110251.1	chromosome 9: 44336348–44344228	6–7	81

at 1:500 dilution for 1 hr at room temperature. Nuclei were counterstained with 4′,6-diamidino-2-phenylindole (DAPI).

In Vivo Injection and Ex Vivo Optical Mapping

All animal procedures were reviewed and approved by the Institutional Animal Care and Use Committee of the Cedars-Sinai Medical Center. For testing of biological pacemaker function in animals implanted with the EBs in vivo, 10–12 whole SHOX2-EBs or GFP-EBs were randomly selected and injected with a 24G needle subepicardially into the left ventricular anterior wall of adult Sprague Dawley female rats upon thoracotomy. At 24 to 48 hr after injection, heart was harvested and retrogradely perfused with normal Tyrode's solution containing 10 μM blebbistatin for 30 min in order to uncouple excitation-contraction, thereby minimizing motion artifacts (Fedorov et al., 2007). The heart was then perfused with di-4-ANEPPS (2 μM; Molecular Probes) for 15 min. Perfusion was made through the aorta, and temperature was continuously maintained at 37°C ± 1°C. During mapping, the heart was positioned in a transparent chamber filled with Tyrode's solution with the injected site facing the optical light path, and the optical signals were recorded from a 5 × 5 mm area at baseline (sinus rhythm) and after complete heart block. Heart block was achieved by mechanically excising the SAN and the AV node. The fluorescence changes were recorded on a 496-diode array mapping system (WuTech).

Single-Cell Electrophysiology

To examine the electrophysiological properties of individual cardiomyocytes derived from mESC, EBs at D6+14 were dispersed into single cells with a protocol modified from a previous report (Zhang et al., 2002). EBs were digested with a nominally calcium-free solution (in mM: NaCl 140, KCl 5.4, KH_2PO_4 1.2, $MgCl_2$ 0.5, HEPES 5, taurine 50, glucose 5.5 [pH = 6.9] with NaOH) containing collagenase B (Roche, 0.5 mg/ml) at 37°C for 50 min followed by digestion with Liberase (Roche, 75 μg/ml) at 35°C for 20 min. Single, whole-cell AP and ionic current measurements were carried out using standard microelectrode whole-cell, patch-clamp technique with an Axopatch 200B amplifier (Molecular Devices) with a sampling rate of 20 kHz and low-pass Bessel-filtered at 5 kHz. Experiments were performed at 33°C ± 1°C. Cells were perfused with a normal Tyrode's solution containing (mM: NaCl 138, KCl 5, $CaCl_2$ 1.8, $MgCl_2$ 0.5, glucose 10, and HEPES 10 [pH = 7.4]) with NaOH. Pipette solution contained (mmol/l) K-glutamate 98, KCl 50, $MgCl_2$ 1.0, HEPES 10, EGTA 2, and K-ATP 5 (pH = 7.2) with KOH. Microelectrodes had tip resistances of 2–4 MΩ when filled with the internal recording solution. Spontaneous APs were recorded with I = 0 mode. Effects of adrenergic and cholinergic agonists on AP firing rate were tested by perfusing cells with Tyrode solution containing isoproterenol (1 μM, Sigma) or acetylcholine (50 nM; Sigma). Data were corrected for the estimated liquid junction potentials (−12.5 mV). The diastolic depolarization rate was determined from the slope of a 20-ms segment after the maximum diastolic potential. Funny currents (I_f) were recorded in a voltage-clamp mode with cells bathed in normal Tyrode's solution containing 1 mM $BaCl_2$ in order to block contaminating inward rectifier K^+ currents (I_{K1}). Holding potential was set at −35 mV, and a family of voltage steps from −135 mV to +35 mV for 1.5 s with 10 mV increment was applied to elicit I_f. The I_f was identified by their time-dependent activation and their sensitivity to ivabradine (10 μM; Sigma-Aldrich).

Similar to the criteria adopted in the human ESC-derived cardiomyocytes (He et al., 2003), the APs were designated ventricular-, atrial- and pacemaker-like cells based on the AP duration and the slope of spontaneous phase 4 depolarization rate. Ordinary ventricular cardiomyocytes exhibit prominent plateau phase, reflected by their slow early repolarization rate (i.e., long APD_{20}) and fast late repolarization rate (short APD_{80}). Accordingly, cells with APD_{20}/APD_{80} >3.0 were categorized to ventricular-like cells. Pacemaker-like APs were designated to cells with fast phase 4 diastolic depolarization rate (>0.04 V/s) and short APD ($APD_{20}/APD_{80} \leq 3.0$). Atrial-like APs were designated to cells with short APD ($APD_{20}/APD_{80} \leq 3.0$) and slow phase 4 diastolic depolarization (≤ 0.04 V/s).

Curve Fitting

The time course of endogenous *Shox2* expression data was processed by nonlinear curve fitting (Figure 2A) with amplitude version of Gaussian peak function with an equation, y = y_0 + A*exp(−0.5 × ((x − xc)/w)^2). Levenberg Marquardt algorithm was used for iteration. The final values for each parameter at the end of the iteration are provided in Table 2.

Table 2. Parameters for the Nonlinear Curve Fitting of the Data in Figure 2A

	Value	SE
y_0	1.88621	0.12281
xc	5.0783	0.23033
w	3.34034	0.3499
A	−1.904	0.13304
Full width at half maximum	7.86591	0.82396
Area	−15.9422	2.2425
Number of points	10	
Degrees of freedom	6	
Reduced chi squared	1.28641	
Adjusted R square	0.96031	

Statistical Analysis

All data are represented as mean ± SEM. Statistical significance was calculated with an unpaired Student's t test. A confidence of $p \leq 0.05$ was considered significant.

SUPPLEMENTAL INFORMATION

Supplemental Information includes five figures, one table, and two movies and can be found with this article online at http://dx.doi.org/10.1016/j.stemcr.2014.11.004.

AUTHOR CONTRIBUTIONS

V.I. designed and carried out all experiments except the single-cell electrophysiology work. W.L. carried out all experiments that relate to the single-cell electrophysiology.

ACKNOWLEDGMENTS

We thank Giselle Galang for adenoviral vector construction, amplification, and purification. Jordan Mak aided in mESC maintenance. The study was supported by the Cedars-Sinai Board of Governors Heart Stem Cell Center, Canadian Institutes of Health Research Fellowship to W.L. and the American Heart Association (12SDG9020030) and National Heart, Lung, and Blood Institute (1R01HL111646-01A1) to H.C.C.

Received: March 4, 2014
Revised: November 20, 2014
Accepted: November 20, 2014
Published: December 18, 2014

REFERENCES

Bakker, M.L., Boukens, B.J., Mommersteeg, M.T., Brons, J.F., Wakker, V., Moorman, A.F., and Christoffels, V.M. (2008). Transcription factor Tbx3 is required for the specification of the atrioventricular conduction system. Circ. Res. *102*, 1340–1349.

Bakker, M.L., Boink, G.J., Boukens, B.J., Verkerk, A.O., van den Boogaard, M., den Haan, A.D., Hoogaars, W.M., Buermans, H.P., de Bakker, J.M., Seppen, J., et al. (2012). T-box transcription factor TBX3 reprogrammes mature cardiac myocytes into pacemaker-like cells. Cardiovasc. Res. *94*, 439–449.

Blaschke, R.J., Hahurij, N.D., Kuijper, S., Just, S., Wisse, L.J., Deissler, K., Maxelon, T., Anastassiadis, K., Spitzer, J., Hardt, S.E., et al. (2007). Targeted mutation reveals essential functions of the homeodomain transcription factor Shox2 in sinoatrial and pacemaking development. Circulation *115*, 1830–1838.

Bleeker, W.K., Mackaay, A.J., Masson-Pévet, M., Bouman, L.N., and Becker, A.E. (1980). Functional and morphological organization of the rabbit sinus node. Circ. Res. *46*, 11–22.

Boheler, K.R., Czyz, J., Tweedie, D., Yang, H.T., Anisimov, S.V., and Wobus, A.M. (2002). Differentiation of pluripotent embryonic stem cells into cardiomyocytes. Circ. Res. *91*, 189–201.

Bonke, F.I. (1973). Electronic spread in the sinoatrial node of the rabbit heart. Pflugers Arch. *339*, 17–23.

Bressan, M., Liu, G., and Mikawa, T. (2013). Early mesodermal cues assign avian cardiac pacemaker fate potential in a tertiary heart field. Science *340*, 744–748.

Cai, C.L., Martin, J.C., Sun, Y., Cui, L., Wang, L., Ouyang, K., Yang, L., Bu, L., Liang, X., Zhang, X., et al. (2008). A myocardial lineage derives from Tbx18 epicardial cells. Nature *454*, 104–108.

Cho, H.C., and Marbán, E. (2010). Biological therapies for cardiac arrhythmias: can genes and cells replace drugs and devices? Circ. Res. *106*, 674–685.

Chong, J.J., Yang, X., Don, C.W., Minami, E., Liu, Y.W., Weyers, J.J., Mahoney, W.M., Van Biber, B., Cook, S.M., Palpant, N.J., et al. (2014). Human embryonic-stem-cell-derived cardiomyocytes regenerate non-human primate hearts. Nature *510*, 273–277.

Christoffels, V.M., Burch, J.B., and Moorman, A.F. (2004). Architectural plan for the heart: early patterning and delineation of the chambers and the nodes. Trends Cardiovasc. Med. *14*, 301–307.

Christoffels, V.M., Mommersteeg, M.T., Trowe, M.O., Prall, O.W., de Gier-de Vries, C., Soufan, A.T., Bussen, M., Schuster-Gossler, K., Harvey, R.P., Moorman, A.F., and Kispert, A. (2006). Formation of the venous pole of the heart from an Nkx2-5-negative precursor population requires Tbx18. Circ. Res. *98*, 1555–1563.

Christoffels, V.M., Grieskamp, T., Norden, J., Mommersteeg, M.T., Rudat, C., and Kispert, A. (2009). Tbx18 and the fate of epicardial progenitors. Nature *458*, E8–E9, discussion E9–E10.

Christoffels, V.M., Smits, G.J., Kispert, A., and Moorman, A.F. (2010). Development of the pacemaker tissues of the heart. Circ. Res. *106*, 240–254.

DiFrancesco, D. (2010). The role of the funny current in pacemaker activity. Circ. Res. *106*, 434–446.

Dubois, N.C., Craft, A.M., Sharma, P., Elliott, D.A., Stanley, E.G., Elefanty, A.G., Gramolini, A., and Keller, G. (2011). SIRPA is a specific cell-surface marker for isolating cardiomyocytes derived from human pluripotent stem cells. Nat. Biotechnol. *29*, 1011–1018.

Espinoza-Lewis, R.A., Yu, L., He, F., Liu, H., Tang, R., Shi, J., Sun, X., Martin, J.F., Wang, D., Yang, J., and Chen, Y. (2009). Shox2 is essential for the differentiation of cardiac pacemaker cells by repressing Nkx2-5. Dev. Biol. *327*, 376–385.

Fedorov, V.V., Lozinsky, I.T., Sosunov, E.A., Anyukhovsky, E.P., Rosen, M.R., Balke, C.W., and Efimov, I.R. (2007). Application of blebbistatin as an excitation-contraction uncoupler for electrophysiologic study of rat and rabbit hearts. Heart Rhythm *4*, 619–626.

Hashem, S.I., Lam, M.L., Mihardja, S.S., White, S.M., Lee, R.J., and Claycomb, W.C. (2013). Shox2 regulates the pacemaker gene program in embryoid bodies. Stem Cells Dev. *22*, 2915–2926.

Hattori, F., Chen, H., Yamashita, H., Tohyama, S., Satoh, Y.S., Yuasa, S., Li, W., Yamakawa, H., Tanaka, T., Onitsuka, T., et al. (2010). Nongenetic method for purifying stem cell-derived cardiomyocytes. Nat. Methods *7*, 61–66.

He, J.Q., Ma, Y., Lee, Y., Thomson, J.A., and Kamp, T.J. (2003). Human embryonic stem cells develop into multiple types of cardiac myocytes: action potential characterization. Circ. Res. *93*, 32–39.

Itzhaki, I., Maizels, L., Huber, I., Zwi-Dantsis, L., Caspi, O., Winterstern, A., Feldman, O., Gepstein, A., Arbel, G., Hammerman, H., et al. (2011). Modelling the long QT syndrome with induced pluripotent stem cells. Nature *471*, 225–229.

Jansen, J.A., van Veen, T.A., de Bakker, J.M., and van Rijen, H.V. (2010). Cardiac connexins and impulse propagation. J. Mol. Cell. Cardiol. *48*, 76–82.

Joyner, R.W., and van Capelle, F.J. (1986). Propagation through electrically coupled cells. How a small SA node drives a large atrium. Biophys. J. *50*, 1157–1164.

Jung, J.J., Husse, B., Rimmbach, C., Krebs, S., Stieber, J., Steinhoff, G., Dendorfer, A., Franz, W.M., and David, R. (2014). Programming and isolation of highly pure physiologically and pharmacologically functional sinus-nodal bodies from pluripotent stem cells. Stem Cell Rep. *2*, 592–605.

Kapoor, N., Liang, W., Marbán, E., and Cho, H.C. (2013). Direct conversion of quiescent cardiomyocytes to pacemaker cells by expression of Tbx18. Nat. Biotechnol. *31*, 54–62.

Kattman, S.J., Witty, A.D., Gagliardi, M., Dubois, N.C., Niapour, M., Hotta, A., Ellis, J., and Keller, G. (2011). Stage-specific optimization of activin/nodal and BMP signaling promotes cardiac differentiation of mouse and human pluripotent stem cell lines. Cell Stem Cell *8*, 228–240.

Kehat, I., Kenyagin-Karsenti, D., Snir, M., Segev, H., Amit, M., Gepstein, A., Livne, E., Binah, O., Itskovitz-Eldor, J., and Gepstein, L. (2001). Human embryonic stem cells can differentiate into myocytes with structural and functional properties of cardiomyocytes. J. Clin. Invest. *108*, 407–414.

Kehat, I., Khimovich, L., Caspi, O., Gepstein, A., Shofti, R., Arbel, G., Huber, I., Satin, J., Itskovitz-Eldor, J., and Gepstein, L. (2004). Electromechanical integration of cardiomyocytes derived from human embryonic stem cells. Nat. Biotechnol. *22*, 1282–1289.

Kleger, A., Seufferlein, T., Malan, D., Tischendorf, M., Storch, A., Wolheim, A., Latz, S., Protze, S., Porzner, M., Proepper, C., et al. (2010). Modulation of calcium-activated potassium channels induces cardiogenesis of pluripotent stem cells and enrichment of pacemaker-like cells. Circulation *122*, 1823–1836.

Kolossov, E., Lu, Z., Drobinskaya, I., Gassanov, N., Duan, Y., Sauer, H., Manzke, O., Bloch, W., Bohlen, H., Hescheler, J., and Fleischmann, B.K. (2005). Identification and characterization of embryonic stem cell-derived pacemaker and atrial cardiomyocytes. FASEB J. *19*, 577–579.

Lakatta, E.G., and DiFrancesco, D. (2009). What keeps us ticking: a funny current, a calcium clock, or both? J. Mol. Cell. Cardiol. *47*, 157–170.

Lian, X., Hsiao, C., Wilson, G., Zhu, K., Hazeltine, L.B., Azarin, S.M., Raval, K.K., Zhang, J., Kamp, T.J., and Palecek, S.P. (2012). Robust cardiomyocyte differentiation from human pluripotent stem cells via temporal modulation of canonical Wnt signaling. Proc. Natl. Acad. Sci. USA *109*, E1848–E1857.

Maltsev, V.A., Rohwedel, J., Hescheler, J., and Wobus, A.M. (1993). Embryonic stem cells differentiate in vitro into cardiomyocytes representing sinusnodal, atrial and ventricular cell types. Mech. Dev. *44*, 41–50.

Maltsev, V.A., Wobus, A.M., Rohwedel, J., Bader, M., and Hescheler, J. (1994). Cardiomyocytes differentiated in vitro from embryonic stem cells developmentally express cardiac-specific genes and ionic currents. Circ. Res. *75*, 233–244.

Mandel, Y., Weissman, A., Schick, R., Barad, L., Novak, A., Meiry, G., Goldberg, S., Lorber, A., Rosen, M.R., Itskovitz-Eldor, J., and Binah, O. (2012). Human embryonic and induced pluripotent stem cell-derived cardiomyocytes exhibit beat rate variability and power-law behavior. Circulation *125*, 883–893.

Michou, A.I., Santoro, L., Christ, M., Julliard, V., Pavirani, A., and Mehtali, M. (1997). Adenovirus-mediated gene transfer: influence of transgene, mouse strain and type of immune response on persistence of transgene expression. Gene Ther. *4*, 473–482.

Mommersteeg, M.T., Hoogaars, W.M., Prall, O.W., de Gier-de Vries, C., Wiese, C., Clout, D.E., Papaioannou, V.E., Brown, N.A., Harvey, R.P., Moorman, A.F., and Christoffels, V.M. (2007). Molecular pathway for the localized formation of the sinoatrial node. Circ. Res. *100*, 354–362.

Müller, M., Stockmann, M., Malan, D., Wolheim, A., Tischendorf, M., Linta, L., Katz, S.F., Lin, Q., Latz, S., Brunner, C., et al. (2012). Ca2+ activated K channels-new tools to induce cardiac commitment from pluripotent stem cells in mice and men. Stem Cell Rep. *8*, 720–740.

Mummery, C.L., Davis, R.P., and Krieger, J.E. (2010). Challenges in using stem cells for cardiac repair. Sci. Transl. Med. *2*, 27ps17.

Mummery, C.L., Zhang, J., Ng, E.S., Elliott, D.A., Elefanty, A.G., and Kamp, T.J. (2012). Differentiation of human embryonic stem cells and induced pluripotent stem cells to cardiomyocytes: a methods overview. Circ. Res. *111*, 344–358.

Norden, J., Greulich, F., Rudat, C., Taketo, M.M., and Kispert, A. (2011). Wnt/β-catenin signaling maintains the mesenchymal precursor pool for murine sinus horn formation. Circ. Res. *109*, e42–e50.

Nunes, S.S., Miklas, J.W., Liu, J., Aschar-Sobbi, R., Xiao, Y., Zhang, B., Jiang, J., Massé, S., Gagliardi, M., Hsieh, A., et al. (2013). Biowire: a platform for maturation of human pluripotent stem cell-derived cardiomyocytes. Nat. Methods *10*, 781–787.

Paige, S.L., Osugi, T., Afanasiev, O.K., Pabon, L., Reinecke, H., and Murry, C.E. (2010). Endogenous Wnt/beta-catenin signaling is required for cardiac differentiation in human embryonic stem cells. PLoS ONE *5*, e11134.

Pelleg, A., Vogel, S., Belardinelli, L., and Sperelakis, N. (1980). Overdrive suppression of automaticity in cultured chick myocardial cells. Am. J. Physiol. *238*, H24–H30.

Schneider, V.A., and Mercola, M. (2001). Wnt antagonism initiates cardiogenesis in Xenopus laevis. Genes Dev. *15*, 304–315.

Shiba, Y., Fernandes, S., Zhu, W.Z., Filice, D., Muskheli, V., Kim, J., Palpant, N.J., Gantz, J., Moyes, K.W., Reinecke, H., et al. (2012). Human ES-cell-derived cardiomyocytes electrically couple and suppress arrhythmias in injured hearts. Nature *489*, 322–325.

Thomson, J.A., Itskovitz-Eldor, J., Shapiro, S.S., Waknitz, M.A., Swiergiel, J.J., Marshall, V.S., and Jones, J.M. (1998). Embryonic stem cell lines derived from human blastocysts. Science *282*, 1145–1147.

Tripathy, S.K., Black, H.B., Goldwasser, E., and Leiden, J.M. (1996). Immune responses to transgene-encoded proteins limit the stability of gene expression after injection of replication-defective adenovirus vectors. Nat. Med. *2*, 545–550.

Van Vliet, P., Wu, S.M., Zaffran, S., and Pucéat, M. (2012). Early cardiac development: a view from stem cells to embryos. Cardiovasc. Res. *96*, 352–362.

Wiese, C., Grieskamp, T., Airik, R., Mommersteeg, M.T., Gardiwal, A., de Gier-de Vries, C., Schuster-Gossler, K., Moorman, A.F., Kispert, A., and Christoffels, V.M. (2009). Formation of the sinus node head and differentiation of sinus node myocardium are independently regulated by Tbx18 and Tbx3. Circ. Res. *104*, 388–397.

Wiese, C., Nikolova, T., Zahanich, I., Sulzbacher, S., Fuchs, J., Yamanaka, S., Graf, E., Ravens, U., Boheler, K.R., and Wobus, A.M. (2011). Differentiation induction of mouse embryonic stem cells into sinus node-like cells by suramin. Int. J. Cardiol. *147*, 95–111.

Willems, E., Spiering, S., Davidovics, H., Lanier, M., Xia, Z., Dawson, M., Cashman, J., and Mercola, M. (2011). Small-molecule inhibitors of the Wnt pathway potently promote cardiomyocytes from human embryonic stem cell-derived mesoderm. Circ. Res. *109*, 360–364.

Wobus, A.M., Wallukat, G., and Hescheler, J. (1991). Pluripotent mouse embryonic stem cells are able to differentiate into cardiomyocytes expressing chronotropic responses to adrenergic and cholinergic agents and Ca2+ channel blockers. Differentiation *48*, 173–182.

Wobus, A.M., Rohwedel, J., Maltsev, V., and Hescheler, J. (1995). Development of cardiomyocytes expressing cardiac-specific genes, action potentials, and ionic channels during embryonic stem cell-derived cardiogenesis. Ann. N Y Acad. Sci. *752*, 460–469.

Xue, T., Cho, H.C., Akar, F.G., Tsang, S.Y., Jones, S.P., Marbán, E., Tomaselli, G.F., and Li, R.A. (2005). Functional integration of electrically active cardiac derivatives from genetically engineered human embryonic stem cells with quiescent recipient ventricular cardiomyocytes: insights into the development of cell-based pacemakers. Circulation *111*, 11–20.

Yamamoto, M., Dobrzynski, H., Tellez, J., Niwa, R., Billeter, R., Honjo, H., Kodama, I., and Boyett, M.R. (2006). Extended atrial conduction system characterised by the expression of the HCN4 channel and connexin45. Cardiovasc. Res. *72*, 271–281.

Zhang, Y.M., Hartzell, C., Narlow, M., and Dudley, S.C., Jr. (2002). Stem cell-derived cardiomyocytes demonstrate arrhythmic potential. Circulation *106*, 1294–1299.

Zhang, J., Wilson, G.F., Soerens, A.G., Koonce, C.H., Yu, J., Palecek, S.P., Thomson, J.A., and Kamp, T.J. (2009). Functional cardiomyocytes derived from human induced pluripotent stem cells. Circ. Res. *104*, e30–e41.

Stem Cell Reports, Volume *4*

Supplemental Information

SHOX2 Overexpression Favors Differentiation of Embryonic Stem Cells into Cardiac Pacemaker Cells, Improving Biological Pacing Ability

Vittoria Ionta, Wenbin Liang, Elizabeth H. Kim, Reza Rafie, Alessandro Giacomello, Eduardo Marbán, and Hee Cheol Cho

Figure S1

CLUSTAL O(1.2.0) multiple sequence alignment: Percent Identity Matrix - created by Clustal2.1

1: gi|7305489|ref|NP_038693.1| 100.00 98.48 (**mouse SHOX2**)
2: gi|14250720|gb|AAH08829.1| 98.48 100.00 (**human SHOX2**)

```
gi|7305489|ref|NP_038693.1|      MEELTAFVSKSFDQKVKEKKEAITYREVLESGPLRGAKEP-GCVEPGRDDRSSPAVRAAG 59
gi|14250720|gb|AAH08829.1|       MEELTAFVSKSFDQKVKEKKEAITYREVLESGPLRGAKEPTGCTEAGRDDRSSPAVRAAG 60
                                 **************************************** **.* **************

gi|7305489|ref|NP_038693.1|      GGGGAGGGGGGGGGGGGGAGGGGAGGGAGGGRSPVRELDMGAAERSREPGSPRLTE---- 115
gi|14250720|gb|AAH08829.1|       GGGGGGG-GGGGGGGGGGVGGGGAGGGAGGGRSPVRELDMGAAERSREPGSPRLTEGRRK 119
                                 ****.** **********.************************************

gi|7305489|ref|NP_038693.1|      --------------------VSPELKDRKDDAKGMEDEGQTKIKQRRSRTNFTLEQLNEL 155
gi|14250720|gb|AAH08829.1|       PTKAEVQATLLLPGEAFRFLVSPELKDRKEDAKGMEDEGQTKIKQRRSRTNFTLEQLNEL 179
                                              *********:******************************

gi|7305489|ref|NP_038693.1|      ERLFDETHYPDAFMREELSQRLGLSEARVQVWFQNRRAKCRKQENQLHKGVLIGAASQFE 215
gi|14250720|gb|AAH08829.1|       ERLFDETHYPDAFMREELSQRLGLSEARVQVWFQNRRAKCRKQENQLHKGVLIGAASQFE 239
                                 ************************************************************

gi|7305489|ref|NP_038693.1|      ACRVAPYVNVGALRMPFQQDSHCNVTPLSFQVQAQLQLDSAVAHAHHHLHPHLAAHAPYM 275
gi|14250720|gb|AAH08829.1|       ACRVAPYVNVGALRMPFQQDSHCNVTPLSFQVQAQLQLDSAVAHAHHHLHPHLAAHAPYM 299
                                 ************************************************************

gi|7305489|ref|NP_038693.1|      MFPAPPFGLPLATLAADSASAASVVAAAAAAKTTSKNSSIADLRLKAKKHAAALGL     331
gi|14250720|gb|AAH08829.1|       MFPAPPFGLPLATLAADSASAASVVAAAAAAKTTSKNSSIADLRLKAKKHAAALGL     355
                                 ********************************************************
```

http://www.ebi.ac.uk/Tools/msa/clustalo/

Figure S2

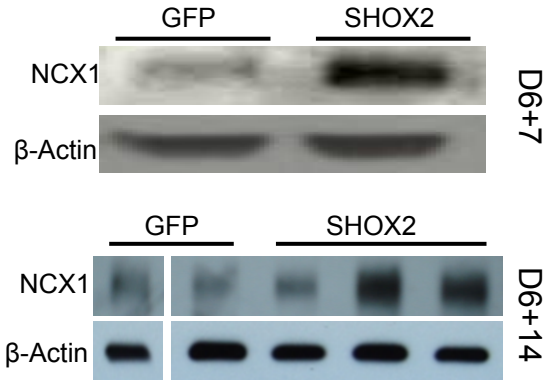

Figure S3

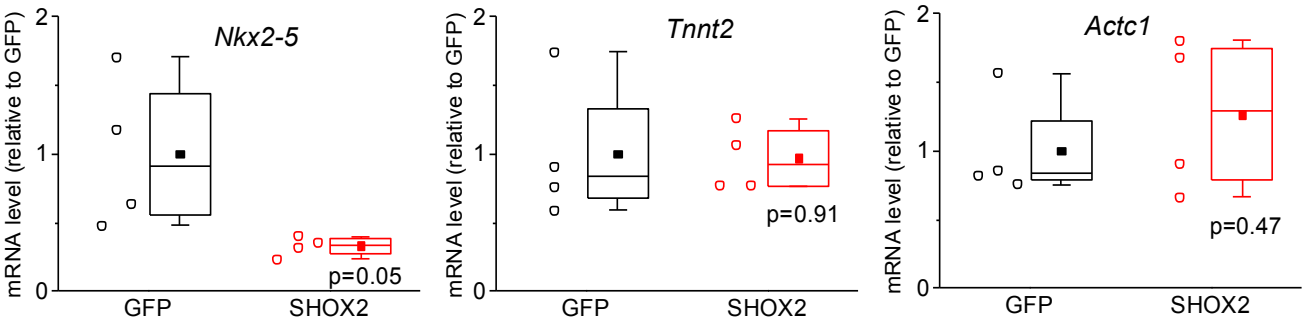
Nkx2-5
mRNA level (relative to GFP)
2
1
0
p=0.05
GFP
SHOX2
Tnnt2
mRNA level (relative to GFP)
2
1
0
p=0.91
GFP
SHOX2
Actc1
mRNA level (relative to GFP)
2
1
0
p=0.47
GFP
SHOX2

Figure S4

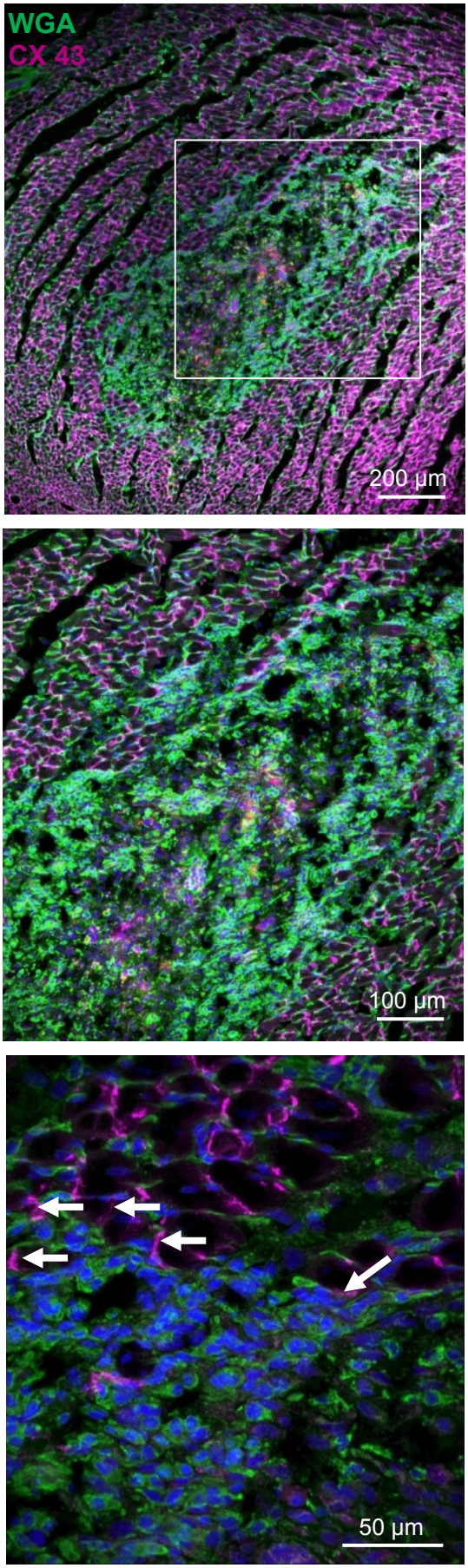

Figure S5

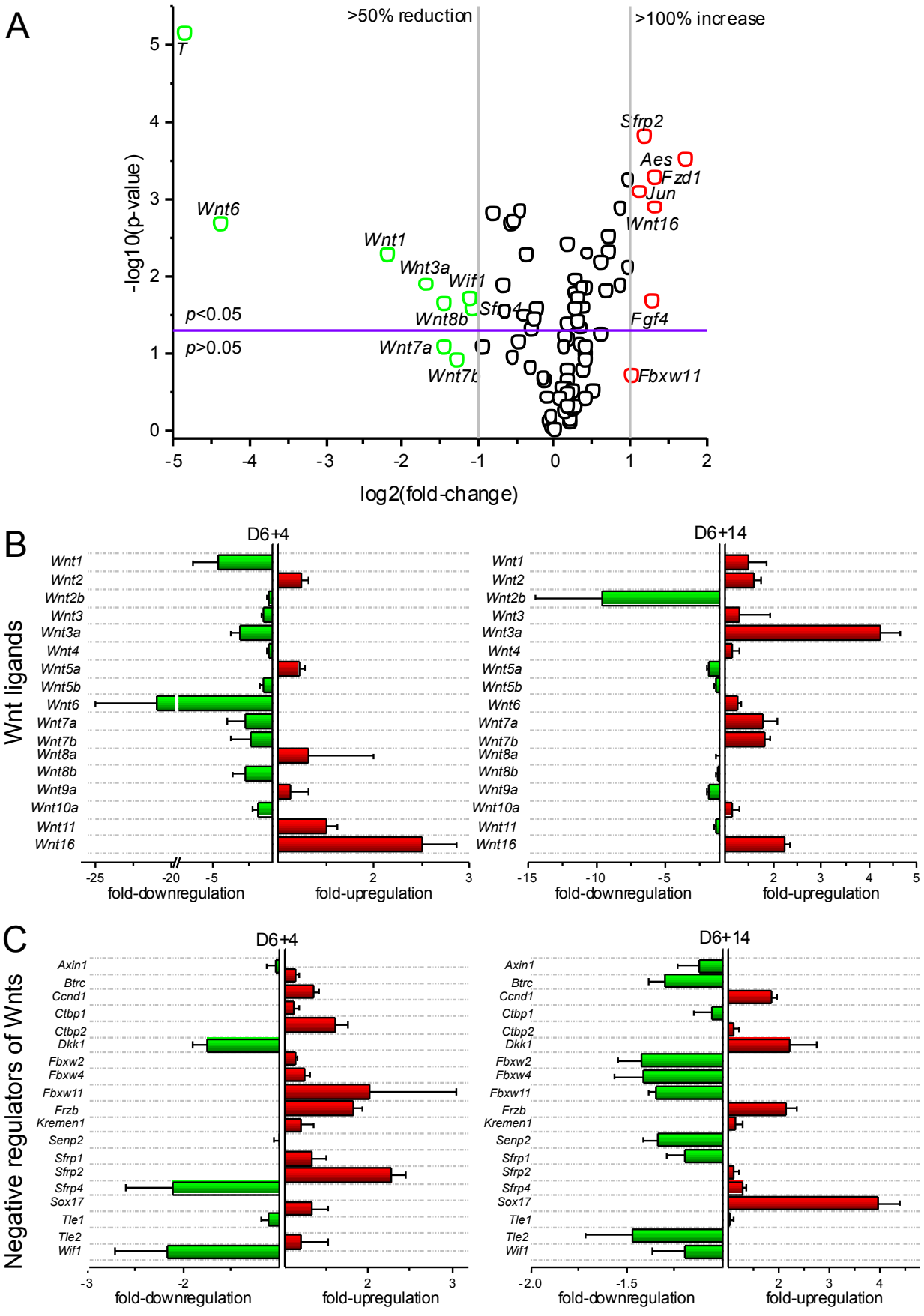
A
>50% reduction
>100% increase
T
Wnt6
Wnt1
Wnt3a
Wif1
Sfo4
Wnt8b
Wnt7a
Wnt7b
Sfrp2
Aes
Fzd1
Jun
Wnt16
Fgf4
Fbxw11
p<0.05
p>0.05
-log10(p-value)
log2(fold-change)
B
Wnt ligands
D6+4
D6+14
Wnt1
Wnt2
Wnt2b
Wnt3
Wnt3a
Wnt4
Wnt5a
Wnt5b
Wnt6
Wnt7a
Wnt7b
Wnt8a
Wnt8b
Wnt9a
Wnt10a
Wnt11
Wnt16
fold-downregulation
fold-upregulation
C
Negative regulators of Wnts
D6+4
D6+14
Axin1
Btrc
Ccnd1
Ctbp1
Ctbp2
Dkk1
Fbxw2
Fbxw4
Fbxw11
Frzb
Kremen1
Senp2
Sfrp1
Sfrp2
Sfrp4
Sox17
Tle1
Tle2
Wif1
fold-downregulation
fold-upregulation

Supplemental data legends

Figure S1, Related to Figure 2. Amino acid sequence alignment between mouse SHOX2 (upper sequence) and human SHOX2 (lower sequence). The alignment indicates >98% SHOX2 protein sequence homology between the two species. The alignment was performed with full-length sequences of the mouse and human homologues.

Figure S2, Related to Figure 3. A Western blot showing NCX1 protein level in GFP- and SHOX2-EBs at the mid (D6+7) and late (D6+14) phases of differentiation. Data are represented as mean ± SEM. All experiments were performed on three independent biological replicates.

Figure S3, Related to Figure 3. Quantitative RT-PCR data on *Nkx2-5* (ventricular marker), *Tnnt2* and *Actc1* (pan-cardiac myocyte markers). All experiments were performed on four independent biological replicates. Data are represented as mean ± SEM.

Figure S4, Related to Figure 4. Gap-junctional expression mediates electrical coupling between a SHOX2-EB and the host myocardium. Using wheat germ agglutinin (WGA, green) as a cell membrane dye, a SHOX2-EB is recognizable as a highly compact structure (top panel). Expression of CX43 co-localizes with WGA, and is found at the boundary between the implanted SHOX2-EBs and the host ventricular myocardium (middle and bottom panels with white arrows).

Figure S5, Related to Discussion. Gene arrays reveal specific and temporal regulation of Wnt signaling in SHOX2-EBs. **A**. A Volcano plot displaying gene expression changes with

>2-fold increase or decrease on vertical lines at 95% confidence level ($p<0.05$) on a horizontal line on D6+4. Most down-regulated genes (green circles) are Wnt ligands while most up-regulated genes (red circles) are Wnt inhibitors. **B**. Although most Wnt ligands are up-regulated at an early differentiation state (D6+4), the trend reverses at a late differentiation stage (D6+14). **C**. Most negative regulators of Wnt signaling are up-regulated at D6+4 (left panel), but the trend reverses at D6+14 (right panel). Fold-regulation = fold-change for values ≥1. Fold-regulation = -1/(fold-change) for values <1. Refer to Table S1 for raw values. Data are represented as mean ± SEM. All experiments were performed on three independent biological replicates.

Movie S1, Related to Figure 4 F, G

An optically-mapped action potential propagation of the rat heart injected with GFP-EBs three days prior to the heart harvest and optical mapping. A nylon suture was tied to the heart adjacent to the EB injection site at the time of surgery in order to locate the site of EB implantation during optical mapping.

Movie S2, Related to Figure 4 F, G

An optically-mapped action potential propagation of the rat heart injected with SHOX2-EBs three days prior to the heart harvest and optical mapping. A nylon suture was tied to the heart adjacent to the EB injection site at the time of surgery in order to locate the site of EB implantation during optical mapping.

Table S1, Related to Figure S5.
Gene array analyses of Wnt pathway-related genes. n=3 for each group.

		Fold-change					
Gene ID	Gene name	**D6+4**	***p*-value**	**D6+7**	***p*-value**	**D6+14**	***p*-value**
NM_010347	*Aes*	3.276	0.000305	1.4264	0.002231	0.7647	0.042676
NM_007462	*Apc*	1.2144	0.010705	0.9756	0.346891	0.8035	0.054744
NM_009733	*Axin1*	0.9631	0.754619	0.946	0.511668	0.894	0.382994
NM_029933	*Bcl9*	1.0804	0.367459	0.9734	0.799399	0.79	0.028516
NM_009771	*Btrc*	1.1212	0.040803	1.0896	0.352936	0.768	0.022354
NM_023465	*Ctnnbip1*	1.1257	0.165815	0.9656	0.570553	1.0246	0.774174
NM_007631	*Ccnd1*	1.3411	0.00498	1.0065	0.870519	1.8413	0.000817
NM_009829	*Ccnd2*	0.6684	0.002094	0.8538	0.389994	1.4282	0.025342
NM_007632	*Ccnd3*	1.2137	0.016936	1.145	0.152217	0.7565	0.010865
NM_146087	*Csnk1a1*	1.2982	0.165425	1.0564	0.362443	0.6245	0.000642
NM_139059	*Csnk1d*	1.1229	0.224413	0.9594	0.138067	0.8102	0.087376
NM_007788	*Csnk2a1*	0.8546	0.026036	1.0055	0.90981	0.7884	0.085497
NM_013502	*Ctbp1*	1.0978	0.27645	1.041	0.737146	0.9437	0.56266
NM_009980	*Ctbp2*	1.6103	0.015091	1.3961	0.019248	1.0995	0.340273
NM_007614	*Ctnnb1*	1.072	0.275689	0.997	0.987086	1.075	0.385025
NM_172464	*Daam1*	1.3314	0.013917	1.2335	0.005867	0.9327	0.476121
NM_178118	*Dixdc1*	1.9493	0.000556	1.0784	0.608085	0.8495	0.005389
NM_010051	*Dkk1*	0.5713	0.001519	0.5461	0.118668	2.2275	0.023196
NM_010091	*Dvl1*	1.2811	0.014497	1.0422	0.729043	0.6231	0.001006
NM_007888	*Dvl2*	0.9119	0.225708	0.9863	0.927445	0.8692	0.107894
NM_177821	*Ep300*	1.1165	0.063855	1.0831	0.067864	0.7988	0.002518
NM_134015	*Fbxw11*	2.0167	0.193919	1.1457	0.014341	0.744	0.000468
NM_013890	*Fbxw2*	1.1353	0.003922	1.1259	0.012562	0.7015	0.006923
NM_013907	*Fbxw4*	1.2278	0.019564	1.1037	0.049432	0.7068	0.023023
NM_010202	*Fgf4*	2.4331	0.02124	4.0619	0.018192	23.8011	0.001387
NM_010235	*Fosl1*	1.6246	0.004717	1.3586	0.009339	0.9044	0.479163
NM_008238	*Foxn1*	1.4115	0.297529	0.8282	0.572989	1.1246	0.483885
NM_008043	*Frat1*	0.6816	0.114305	0.78	0.061114	0.9111	0.446768
NM_011356	*Frzb*	1.8161	0.001281	2.324	0.003164	2.1508	0.003332
NM_008045	*Fshb*	1.1587	0.789193	0.8355	0.595354	0.8794	0.832505

NM_021457	*Fzd1*	2.5056	0.000515	1.4636	0.018939	1.2648	0.070754
NM_020510	*Fzd2*	1.1463	0.321017	0.9494	0.722192	1.0257	0.782463
NM_021458	*Fzd3*	0.8139	0.047049	0.8241	0.134851	1.0174	0.746618
NM_008055	*Fzd4*	1.1508	0.718765	1.2695	0.148967	0.7949	0.01157
NM_022721	*Fzd5*	0.9676	0.661034	0.7397	0.082845	1.5543	0.002281
NM_008056	*Fzd6*	1.3336	0.101544	0.9021	0.313787	1.3387	0.01821
NM_008057	*Fzd7*	0.9697	0.92192	1.0972	0.267028	0.8883	0.138028
NM_008058	*Fzd8*	1.953	0.007732	1.7436	0.049979	0.8005	0.104091
NM_019827	*Gsk3b*	1.2872	0.025103	1.0901	0.438091	0.962	0.299319
NM_010591	*Jun*	2.1682	0.000794	1.4502	0.000859	0.705	0.003064
NM_032396	*Kremen1*	1.1876	0.294575	0.9352	0.632573	1.1396	0.300324
NM_010703	*Lef1*	0.6889	0.001911	0.8343	0.345297	2.0225	0.007239
NM_008513	*Lrp5*	1.1251	0.319753	1.2195	0.108942	1.0907	0.424482
NM_008514	*Lrp6*	1.0996	0.059099	1.1644	0.051199	0.756	0.019297
NM_010849	*Myc*	1.248	0.076415	1.0485	0.651399	1.2624	0.054826
NM_027280	*Nkd1*	1.0935	0.567878	1.3194	0.098683	0.663	0.012796
NM_008702	*Nlk*	0.9397	0.369744	0.9093	0.246901	0.7538	0.107873
NM_011098	*Pitx2*	1.5275	0.057242	0.8136	0.187599	0.8708	0.238799
NM_023638	*Porcn*	0.7232	0.072025	1.0215	0.828221	0.7938	0.068313
NM_019411	*Ppp2ca*	1.0867	0.08461	1.098	0.054489	0.9103	0.266752
NM_016891	*Ppp2r1a*	1.0544	0.374698	1.1267	0.096795	0.8096	0.147929
NM_009358	*Ppp2r5d*	1.1789	0.51911	1.0079	0.903682	0.8583	0.390821
NM_028116	*Pygo1*	1.639	0.003099	0.9993	0.972997	0.663	0.006465
NM_133955	*Rhou*	0.7672	0.005102	0.5258	0.01207	0.9554	0.137197
NM_029457	*Senp2*	0.997	0.934238	0.9141	0.214292	0.7497	0.009738
NM_013834	*Sfrp1*	1.3329	0.08424	1.4142	0.07399	0.8364	0.069534
NM_009144	*Sfrp2*	2.2658	0.000153	1.6819	0.02889	1.1079	0.349366
NM_016687	*Sfrp4*	0.4738	0.026127	1.5439	0.18759	1.268	0.022702
NM_012030	*Slc9a3r1*	0.7494	0.031734	0.6118	0.000382	0.7057	0.04961
NM_011441	*Sox17*	1.3259	0.120226	1.4035	0.189761	3.964	0.000659
NM_009309	*T*	0.0346	0.000007	0.301	0.565313	1.5152	0.271885
NM_009332	*Tcf7l1*	1.2544	0.046597	1.046	0.607949	1.0117	0.898628
NM_009331	*Tcf7*	0.7296	0.00142	0.6949	0.060118	1.3977	0.006177
NM_011599	*Tle1*	0.9004	0.206392	0.8921	0.125742	1.0426	0.594168
NM_019725	*Tle2*	1.2016	0.482473	1.224	0.406355	0.6799	0.086491

NM_011915	*Wif1*	0.4625	0.018657	0.2066	0.011536	0.836	0.285105
NM_018865	*Wisp1*	1.8179	0.012896	1.4427	0.054786	0.932	0.561327
NM_021279	*Wnt1*	0.2188	0.005193	0.459	0.14925	1.4756	0.219157
NM_009518	*Wnt10a*	0.5236	0.079737	0.8329	0.342212	1.1638	0.221677
NM_009519	*Wnt11*	1.5108	0.006588	1.736	0.000719	0.8108	0.075589
NM_053116	*Wnt16*	2.5	0.001249	1.6603	0.053803	2.2347	0.000409
NM_023653	*Wnt2*	1.2397	0.039224	1.5205	0.160178	1.5962	0.019977
NM_009520	*Wnt2b*	0.8008	0.148713	0.9408	0.932869	0.1043	0.089598
NM_009521	*Wnt3*	0.6335	0.028589	1.0931	0.9563	1.2865	0.360366
NM_009522	*Wnt3a*	0.3138	0.012517	0.7184	0.546478	4.2342	0.000618
NM_009523	*Wnt4*	0.8219	0.036449	0.5839	0.125295	1.1525	0.267361
NM_009524	*Wnt5a*	1.2158	0.026522	0.8167	0.131291	0.5536	0.000443
NM_009525	*Wnt5b*	0.6283	0.013257	0.963	0.96567	0.7658	0.028643
NM_009526	*Wnt6*	0.0477	0.002126	0.1467	0.054278	1.2761	0.005464
NM_009527	*Wnt7a*	0.3637	0.083025	0.363	0.042724	1.7864	0.048506
NM_009528	*Wnt7b*	0.4079	0.117873	0.4835	0.222231	1.8264	0.000781
NM_009290	*Wnt8a*	1.326	0.391264	0.9234	0.908552	0.9882	0.864273
NM_011720	*Wnt8b*	0.3657	0.021851	1.5873	0.322283	0.9385	0.866807
NM_139298	*Wnt9a*	1.1291	0.488897	0.7314	0.145013	0.581	0.025923

WNT Signaling Pathways:

Canonical: Aes (TLE/Groucho*), Apc, Axin1, Bcl9 , Csnk1a1, Csnk1d, Csnk2a1, Ctbp1, Ctbp2, Ctnnb1, Ctnnbip1 (ICAT), Dixdc1, Dkk1, Dvl1, Dvl2, Ep300, Frat1, Fzd1, Fzd2, Fzd3, Fzd4, Fzd5, Fzd6, Fzd7, Fzd8, Gsk3b, Lef1, Lrp5, Lrp6, Nkd1, Porcn, Ppp2ca, Ppp2r1a, Ppp2r5d, Pygo1, Senp2, Sfrp1, Sfrp2, Sfrp4, Sox17, Tcf7l1, Tcf7, Wif1, Wnt1, Wnt10a, Wnt16, Wnt2, Wnt2b, Wnt3, Wnt3a, Wnt4, Wnt6, Wnt7a, Wnt7b, Wnt8a, Wnt8b*.

Planar Cell Polarity (PCP): *Daam1, Dvl1, Dvl2, Nkd1, Rhou, Wnt9a*.

Wnt/Ca^{2+}: *Fzd2, Wnt1, Wnt10a, Wnt11, Wnt16, Wnt2, Wnt2b, Wnt3, Wnt3a, Wnt4, Wnt5a, Wnt5b, Wnt6, Wnt7a, Wnt7b, Wnt8a, Wnt9a*.

WNT Signaling Negative Regulation: *Apc, Axin1, Btrc (bTrCP), Ccnd1, Ctbp1, Ctbp2, Ctnnbip1 (ICAT), Dkk1, Fbxw11, Fbxw2, Fbxw4, Frzb (FRP-3), Kremen1, Lrp6, Nlk, Nkd1, Senp2, Sfrp1, Sfrp2, Sfrp4, Sox17, Tle1, Tle2, Wif1*.

WNT Signaling Target Genes: *Btrc (bTrCP), Ccnd1, Ccnd2, Ccnd3, Fosl1 (FRA-1), Jun, Myc, Pitx2, T (Brachyury)*.

Developmental Processes:

Cell Fate: *Ctnnb1, Dkk1, Wnt1, Wnt3, Wnt3a*.

Tissue Polarity: *Fzd2, Fzd3, Fzd5, Fzd6*.

Cell Growth & Profileration: *Apc, Ccnd1, Ccnd2, Ccnd3, Ctbp1, Ctbp2, Ctnnb1, Ctnnbip1 (ICAT), Ep300, Fgf4, Fosl1, Foxn1, Fshb, Fzd3, Jun, Lrp5, Myc, Ppp2ca, Ppp2r1a, T (Brachyury), Wisp1, Wnt3a*.

Cell Migration: *Apc, Dkk1, Lrp5, Lrp6, Wnt1*.

Cell Cycle: *Apc, Btrc (bTrCP), Ccnd1, Ccnd2, Ccnd3, Ctnnb1, Ep300, Fosl1, Jun, Myc, Rhou, Tcf7l1*.

Cellular Homeostasis: *Apc, Fzd2, Jun, Myc, Slc9a3r1*.